



Available online at www.sciencedirect.com



Applied Acoustics 00 (2021) 1–19

Applied
Acoustics

A Kalman-based Doppler Tracking Algorithm for Underwater Acoustic Spread Spectrum Communications

Dajun Sun^{a,b,c}, Xiaoping Hong^{a,b,c}, Hongyu Cui^{a,b,c,*}

^aCollege of Underwater Acoustic Engineering, Harbin Engineering University, Harbin 150001, China.

^bAcoustic Science and Technology Laboratory, Harbin Engineering University, Harbin 150001, China.

^cKey Laboratory of Marine Information Acquisition and Security (HEU), Ministry of Industry and Information Technology, Harbin 150001, China

Abstract

This paper investigates a method that dynamically tracks and compensates the Doppler spread of the spread spectrum signal in underwater acoustic communications. Due to the ultra-wideband property of the underwater acoustic signal, the Doppler spread is manifested as frequency shifting and time scaling, dilation, or compression. The accurate estimation of the waveform dilation/compression in the time domain corresponds to the Doppler spread. A finer Doppler spread based on the passband signal can be discriminated due to the higher sampling rate than the baseband signal. In this paper, a novel Kalman-based Doppler tracking and compensation algorithm that operates on *passband* for underwater acoustic spread spectrum signal is addressed in a symbol-by-symbol fashion. The received signal is firstly correlated with the local passband reference signal to obtain the de-spreaded passband signal, and then a fractional time delay estimation on the passband signal by cosine waveform approximation is performed to achieve a higher accuracy of time delay estimation. The time difference of the two adjacent symbols is used as the input of the Kalman filter based on the delay-Doppler equation to estimate the instant Doppler factor sequentially. This algorithm adaptively changes the local reference signal based on the filtered Doppler factor for compensating magnitude distortion induced by the velocity variation. Both numerical simulation and experimental data analysis are presented to demonstrate the usability of the proposed algorithm.

Keywords: underwater acoustic communications, spread spectrum, passband Doppler tracking, Kalman filter

1. Introduction

Spread spectrum is a modulation technique that makes the transmitted signal wider in bandwidth than the information bandwidth by modulating the message bits with a pseudorandom sequence. The intentional interference as multipath and unintentional interference such as single tone with high intensity is substantially reduced after the de-spread of the spread spectrum modulation in the receiver, which is widely used in the underwater acoustic physical layer and networking [1, 2].

In underwater acoustic communications, the signal propagates at a slow speed of approximately 1500 m/s, and propagation occurs over multiple paths. Delay spread over ten or even hundreds of milliseconds results in multipath spread distortion, and motion between the transmitter and the receiver creates significant Doppler spread [3, 4]. Both interferences of multipath spread and Doppler spread impose the primary challenge on the design of the receiver. The spread spectrum signal has good auto-correlation property. Each path can be discriminated specifically as long as the

*Corresponding author

Email address: cuihongyu@hrbeu.edu.cn (Hongyu Cui)

duration of the spread sequence is longer than the maximum delay spread. The multipath structure can even benefit underwater spread spectrum communications using a RAKE or passive phase conjugation receiver [5]. Since the underwater acoustic channel is characterized as ultra-wideband and dynamic in nature, Doppler spread could change significantly within the transmission packet when its duration is sufficiently long, especially for the spread spectrum signal that modulates information bits with a long spread sequence. The rapid change of Doppler spread within a data packet results in severe magnitude distortion of correlation and significant performance loss of spread spectrum transmission scheme.

In the field of underwater spread spectrum communications, how to improve the performance of communication systems in severe Doppler spread is a major concern for the design of viable receivers. A widely discussed solution that attempts to fully recover the channel and achieve exact symbol synchronization based on chip-level equalization integrated with the phase lock loop (PLL) is addressed in [6]. However, high signal-to-noise (SNR) signals are required [1]. When the Doppler spread is nearly constant within a data packet, block estimation, such as measuring the time difference of Doppler-insensitive signal pulse pair between packet head and tail [7], is practical. However, it is not valid for many cases, especially for spread spectrum signals with a long transmission time. Another widely used solution is based on computing the cross-ambiguity function (CAF) [8]. The match filter bank of different Doppler offsets is required to realize Doppler estimation for each symbol [9]. Each bank replica is of a different sample length that corresponds to different Doppler offsets. However, this kind of method is computationally intensive due to a large number of Doppler offsets.

In this paper, we extend the previous work that addresses the issue of Doppler tracking of spread spectrum signal [10] to a Kalman filter framework to achieve better performance. Due to the ultra-wideband property of the underwater acoustic channel, the Doppler spread is manifested not only as frequency shifting but also as time scaling, dilation or compression. The accurate estimation of waveform dilation/compression in the time domain corresponds to the Doppler spread. Since the passband signal has a higher sampling rate than the baseband signal, a finer Doppler estimation is achieved where the sampling rate of the receiver limits its resolution [11]. A fractional delay estimator of high accuracy operated on passband correlation output is then used as the input of Kalman filter to update delay and Doppler estimates based on the constant acceleration model. Symbol synchronization and phase rotation compensation are therefore performed based on delay and Doppler estimates. To mitigate the magnitude distortion induced by Doppler spread, the local reference signal is changed adaptively based on the filtered Doppler estimate. Moreover, the delay prediction of the Kalman filter is used to refine the delay measurement. The contributions of this paper are as follows:

1. The fractional delay estimator of high accuracy is employed to estimate Doppler offset. The Doppler estimation is isolated with symbol decision and does not have the problem of error propagation as decision feedback equalization integrated with PLL. The delay prediction of the Kalman filter is used to refine the delay measurement, which is useful when the close multipath occurs.
2. A Kalman filter framework that models the Doppler spread induced by the motion of the transceivers as constant acceleration is proposed to achieve delay-Doppler estimation. The filtered Doppler estimate is therefore used to compensate phase rotation and generate the local reference signal to mitigate magnitude distortion accordingly.
3. Both numerical simulation and experimental data analysis demonstrate the usability of the proposed Kalman-based Doppler tracking algorithm.

This paper is organized as follows. Section 2 presents the fundamentals of the system model. A detailed description of the proposed algorithm is followed in section 3. Simulation results and experimental data analysis are presented in sections 4 and 5, respectively. Finally, section 6 summarizes the whole paper.

2. System Model

2.1. Transmitted Signal

Since the differential modulation does not require training sequences and is robust against the carrier phase ambiguity, the differential BPSK (DBPSK) modulation scheme is considered herein. The differential encoded symbols, $\{b[n]\}$, with a length of N are described as

$$b[n] = a[n] b[n - 1] \quad (1)$$

where $\{a[n]\}$ denote the information symbols.

Let T_b denote the symbol interval, and f_c denote the carrier frequency, and the transmitted spread spectrum signal is described as

$$s(t) = \Re \left\{ \sum_{n=0}^{N-1} b[n] \varphi(t - nT_b) e^{j2\pi f_c t} \right\} \quad (2)$$

where $\varphi(t)$ represents the characterized waveform and is defined as the convolution of spread sequences and pulse shape filter as shown in eq. (3).

$$\varphi(t) = \sum_{m=0}^{L-1} c[m] g(t - mT_c) \quad (3)$$

where $\{c[m]\}$ denote the spread sequences with a length of L , T_c denotes the chip interval, and $g(t)$ denotes the pulse shaping filter, e.g., a rectangle window in this paper.

2.2. Channel Model

A non-uniform path speed model that emphasizes the channel physical propagation properties is considered here [12]. The UWA channel is characterized as different paths that have different amplitudes, time delays, and Doppler spreads. The channel impulse response is given by

$$h(t, \tau) = \sum_{p=0}^{P-1} h_p(t) \delta(\tau - \tau_p(t)) \quad (4)$$

where P is the channel length, and $h_p(t)$ and $\tau_p(t)$ are the amplitude and time delay of path p , respectively.

The time delay of p , represented by $\tau_p(t)$, is defined as

$$\tau_p(t) = \frac{d_p(t)}{c} = t - \alpha_p(t) \quad (5)$$

where c is the underwater sound speed, $d_p(t)$ is the distance that the signal, transmitted at time $\alpha_p(t)$, travels before reaching the receiver. Assume the amplitude is constant within a data packet, the channel impulse response in eq. (4) is approximated as

$$h(t, \tau) \approx \sum_{p=0}^{P-1} h_p \delta(\tau - \tau_p(t)) \quad (6)$$

2.3. Received Signal

The received spread spectrum signal is represented as the convolution of the transmitted signal and the channel impulse response, and is calculated as

$$r(t) = s(t) * h(t, \tau) + \omega(t) = \sum_{p=0}^{P-1} h_p s(t - \tau_p(t)) + \omega(t) \quad (7)$$

where $\omega(t)$ represents the additive white Gaussian noise.

Substituting eq. (2) into the above equation, the received signal can be rewritten as

$$r(t) = \Re \left\{ \sum_{n=0}^{N-1} b[n] \sum_{p=0}^{P-1} h_p \varphi(t - \tau_p(t) - nT_b) e^{j2\pi f_c(t - \tau_p(t))} \right\} + \omega(t) \quad (8)$$

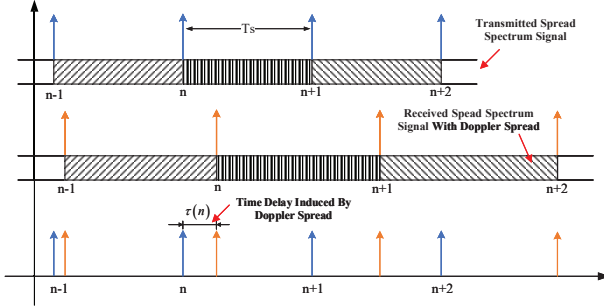


Figure 1. The schematic diagram of the joint delay-Doppler estimation for DSSS signal.

3. The Proposed Algorithm

After describing the system in Section 2, the proposed Kalman-based Doppler tracking algorithm for underwater acoustic spread spectrum signal is presented in this section. As shown in Fig. 1, the time delay of spread spectrum signal induced by Doppler spread at symbol n and path p , $\tau_p[n] = \tau_p(n\Delta t)$, is expressed as

$$\tau_p[n] = \frac{d_p[n]}{c} \quad (9)$$

where $d_p[n] = d_p(n\Delta t)$ denotes the corresponding distance that signal travels from transmitter to the receiver through path p . As in [13, 14], the distance $d_p[n]$ can be approximated using Taylor series by a polynomial of order 3, i.e., constant acceleration (CA) model, as

$$d_p[n] = d_p[n-1] + v_p[n-1]\Delta t + \frac{1}{2}a_p[n-1]\Delta t^2 + \frac{1}{6}g\Delta t^3 \quad (10)$$

where $d_p[n-1]$, $v_p[n-1]$, and $a_p[n-1]$ are the distance, relative velocity, and acceleration at symbol $n-1$, respectively. $\Delta t = T_b$ denotes the observing interval, and g is the acceleration variance and described as a Gaussian distribution with the parameter of $N(0, \sigma_g^2)$ to tolerate the error of the channel model induced by Doppler spread. Assuming the duration of the spread sequence is longer than the maximum delay spread, each path can be discriminated specifically and tracked individually. Therefore, the subscript p is dropped to discuss the proposed algorithm without loss of generality.

Substituting eq. (10) into eq. (9), the time delay of the n th symbol is calculated as

$$\tau[n] = \tau[n-1] + v[n-1]\frac{\Delta t}{c} + a[n-1]\frac{\Delta t^2}{2c} + g\frac{\Delta t^3}{6c} \quad (11)$$

Eq. (11) and derivative of the distance described in eq. (10) are then organized in the form of a matrix as the state transition equation of the Kalman-based delay-Doppler estimator.

$$\mathbf{x}(n) = \mathbf{A}\mathbf{x}(n-1) + \mathbf{w}(n) \quad (12)$$

where

$$\mathbf{x}(n) = \begin{bmatrix} \tau[n] \\ v[n] \\ a[n] \end{bmatrix}, \mathbf{A} = \begin{bmatrix} 1 & \frac{\Delta t}{c} & \frac{\Delta t^2}{2c} \\ 0 & 1 & \Delta t \\ 0 & 0 & 1 \end{bmatrix}, \mathbf{w}(n) = \begin{bmatrix} \frac{\Delta t^3}{6c} \\ \frac{\Delta t^2}{2} \\ \Delta t \end{bmatrix} \cdot g \quad (13)$$

where $\mathbf{x}(n)$ denotes the state vector containing the instant delay estimate, velocity estimate and acceleration estimate respectively. Matrix \mathbf{A} denotes the state transition matrix. Vector $\mathbf{w}(n)$ denotes the process noise vector that describes the error of the state transition equation, and its covariance matrix \mathbf{Q} is calculated as

$$\mathbf{Q} = E[\mathbf{w}(n)\mathbf{w}^T(n)] = \begin{bmatrix} \frac{\Delta t^6}{36c^2} & \frac{\Delta t^5}{12c} & \frac{\Delta t^4}{6c} \\ \frac{\Delta t^5}{12c} & \frac{\Delta t^4}{4} & \frac{\Delta t^3}{2} \\ \frac{\Delta t^4}{6c} & \frac{\Delta t^3}{2} & \Delta t^2 \end{bmatrix} \sigma_g^2 \quad (14)$$

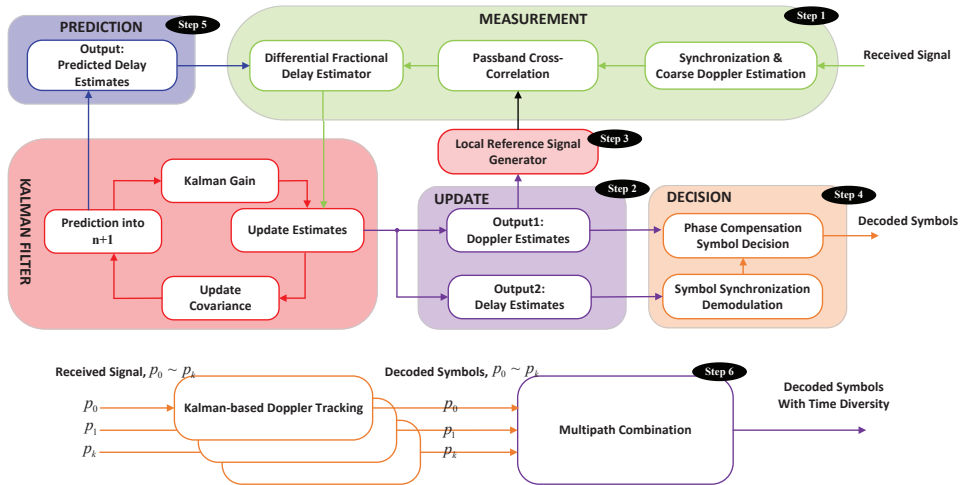


Figure 2. Structure of the proposed Kalman-based Doppler tracking algorithm.

The estimated time delay of spread spectrum signal at symbol n is represented as

$$z[n] = \tau[n] + \omega[n] \quad (15)$$

where $z[n]$ denotes the output of the fractional delay estimator and is used as the input of the Kalman filter. $\tau[n]$ denotes the actual time delay at symbol n , and $\omega[n]$ denotes the error item of delay estimator in the form of Gaussian noise with the parameter of $N(0, \sigma_\omega^2)$.

The delay measurement of the Kalman-based delay-Doppler estimation incorporated with state vector $\mathbf{x}(n)$ is described as

$$z(n) = \mathbf{H}\mathbf{x}(n) + \omega(n) \quad (16)$$

where $\mathbf{H} = [1, 0, 0]^T$ is the measurement matrix that maps the state vector to the delay measurement.

Herein, the parameter required by the Kalman-based delay Doppler estimation are presented above and described as the parameter set, $\Lambda = \{\mathbf{x}, z, \mathbf{H}, \mathbf{A}, \mathbf{Q}, \sigma_\omega^2\}$.

In practical application, underwater maneuvering targets and vessels move much slower than land-based and airborne maneuvering targets. Therefore, the CA model is always approximately suitable for the majority of maneuvering scenarios underwater. By considering the model mismatch in the Kalman filter, the process noise covariance \mathbf{Q} is used to control the tolerance of model mismatch [15], and the larger \mathbf{Q} is equivalent to considering more significant uncertainty in the state equations.

Fig. 2 shows the structure of the proposed Kalman-based Doppler tracking algorithm. As shown, the received signal is firstly synchronized based on delay-Doppler two-dimensional searching, and the coarse Doppler estimation is performed. The synchronized signal is then correlated with the local passband reference signal to generate a cross-correlated passband waveform. The fractional delay estimator is performed to measure the delay of adjacent two symbols. The delay measurements drive the Kalman filter to produce delay and Doppler estimates. The filtered Doppler estimate is used to generate the reference signal for the following symbol adaptively and mitigate the phase rotation induced by residual Doppler offset. The delay estimate is used for symbol synchronization, and the symbol decision integrated with phase compensation is then performed to produce the decoded bits. The fractional delay estimator accepts the predictive delay estimate as the input for dynamic estimating and filtering to refine the delay estimates.

3.1. Delay Measurement

As shown in Fig. 2, the received signal is first synchronized based on a match filter bank where different branches contain reference signals of different sampling lengths. Each branch corresponds to a different Doppler offset. In

this stage, both synchronization and coarse Doppler estimation is performed by peak detection along with the delay-Doppler profile and is described as

$$[\tilde{\tau}_0, \tilde{\alpha}_0] = \arg \max_{\tau \in \tau, \alpha \in \alpha} \left| \int_{-\infty}^{+\infty} r(t) s^*((1 + \alpha)t + \tau) dt \right| \quad (17)$$

where α denotes the Doppler offset, i.e., the ratio of instant velocity to the underwater sound speed. $s((1 + \alpha)t)$ denotes the local passband reference signal with specific Doppler offset.

Table 1. Subfunction: Fractional Time Delay Estimation

Subfunction: $z(n) = \text{fracDelayEst}(R_n(\tau), \hat{\tau}_n, \hat{\tau}_{n+1}, \tau_{pre})$	
1:	$\tilde{\tau}_n = f_D(R_n(\tau), \hat{\tau}_n, \tau_{pre})$
2:	$\tilde{\tau}_{n+1} = f_D(R_n(\tau), \hat{\tau}_{n+1}, \tilde{\tau}_n + (1 + \tilde{\alpha}_n) T_b)$
3:	$z(n) = \sum_{i=0}^n \tilde{\tau}_{i+1} - \tilde{\tau}_i$
Subfunction: $\tilde{\tau} = f_D(r(\tau), \hat{\tau}, \tau_{pre})$	
1:	$\text{TH} = 0.5 \max(r(\tau))$
2:	$[\text{pVec}, \tau\text{Vec}] = \text{findpeaks}(\Re\{r(\tau)\} , \text{TH})$
3:	if $ \hat{\tau} - \tau_{pre} < 1/(2f_c)$
4:	$\tau_2 = \arg \min_{\tau \in \tau\text{Vec}} \tau - \tau_{pre} $
5:	else
6:	$\tau_2 = \arg \min_{\tau \in \tau\text{Vec}} \tau - \hat{\tau} $
7:	end if
8:	$\tau_1 = \tau_2 - t_s, \tau_3 = \tau_2 + t_s$
9:	$r_1 = r(\tau_1), r_2 = r(\tau_2), r_3 = r(\tau_3)$
10:	$\omega = \cos^{-1}((r_1 + r_3)/2r_2)/t_s$
11:	$\phi = \tan^{-1}\left(\frac{r_2 \cos(\omega\tau_1) - r_1 \sin(\omega\tau_2)}{r_1 \sin(\omega\tau_2) - r_2 \sin(\omega\tau_1)}\right)$
12:	$k = \lceil (\omega\tau_1 - \phi)/\pi \rceil$
13:	$\tilde{\tau} = (k\pi + \phi)/\omega$

Assume the Doppler offset is constant within a symbol interval and denotes as α_n at symbol n . The proposed algorithm works in a symbol-by-symbol fashion, with each period spanning two symbol intervals. The received signal at the n th symbol is described as

$$r_n(t) = \Re \left\{ \sum_{k=n}^{n+1} h_{0b}[k] \varphi((1 - \alpha_k)t - nT_b) e^{j2\pi f_c(1 - \alpha_k)t} \right\} + n(t) \quad (18)$$

The local passband reference signal is represented as

$$s_{\tilde{\alpha}_n}(t) = \varphi((1 - \tilde{\alpha}_n)t) e^{j2\pi f_c(1 - \tilde{\alpha}_n)t} \quad (19)$$

where $\tilde{\alpha}_n$ denotes the the Doppler offset generated by the local reference signal generator.

The cross-correlation of the received signal and the local passband reference signal is therefore calculated as

$$R_n(\tau) = r_n(t) * s_{\tilde{\alpha}_n}(t) \approx \sum_{k=n}^{n+1} h_{0b}(k) R_c(\tau - \tau_k) e^{j2\pi f_c(1 + \alpha_k - \tilde{\alpha}_n)(\tau - \tau_k)} \quad (20)$$

where $R_c(\tau)$ denotes the auto-correlation function of the characterized waveform that corresponds to the designated spread sequence.

In underwater acoustic channels, the Doppler spread is manifested as frequency shifting and time scaling, compression, or dilation. The delay estimate is used as Kalman-based delay-Doppler estimation input, and a delay estimation

of higher resolution corresponds to a more refined Doppler estimate and quicker convergence. Since the passband signal has a higher sampling rate than the baseband signal, finer delay estimates can be achieved [11]. Based on this idea, a modified fractional time delay estimator, originated from delay estimation for pulse signal [16], is deployed to measure the time delay [10]. The modified fractional time delay estimator is generalized as Table 1 and described as

$$z(n) = \text{fracDelayEst}(R_n(\tau), \hat{\tau}_n, \hat{\tau}_{n+1}, \tau_{pre}) \quad (21)$$

where τ_{pre} denotes the delay prediction of the Kalman filter shown in Fig. 2 and is used to refine the delay estimates. $\hat{\tau}_k$ denotes the time delay that corresponds to the peak of k th symbol's correlation envelop, and is described as

$$\hat{\tau}_k = \max_{\tau \in \tau_k} |R_n(\tau)|, k = n, n + 1 \quad (22)$$

The kernel behind the fractional time delay estimator is that the cross-correlated passband waveform of the spread spectrum signal is approximated as a cosine function near the correlation peak for each symbol. A higher resolution of delay estimate is achieved by interpolation. Here, $\hat{\tau}_n$ and $\hat{\tau}_{n+1}$ are used as the interval of finding the correlation peak. To refine the delay estimates, the delay prediction generated by the Kalman filter τ_{pre} is used. The delay prediction can improve the tracking when the close multipath occurs.

3.2. Delay Doppler Updates

As shown in Fig. 2, the Kalman filter is driven by the delay measurement, $z(n)$, and updates the delay Doppler estimates accordingly. The output of the Kalman filter is described as

$$\hat{\mathbf{x}}(n | n) = \hat{\mathbf{x}}(n | n - 1) + \mathbf{K}(n) [z(n) - \mathbf{H}^T \hat{\mathbf{x}}(n | n - 1)] \quad (23)$$

where $\hat{\mathbf{x}}(n | n - 1)$ is the previously predicted state vector, $\hat{\mathbf{x}}(n | n)$ is the currently estimated state vector that contains the delay Doppler estimates, and $\mathbf{K}(n)$ is the Kalman gain matrix, and calculated by

$$\mathbf{K}(n) = \mathbf{P}(n | n - 1) \mathbf{H} [\mathbf{H} \mathbf{P}(n | n - 1) \mathbf{H}^T + \sigma_\omega^2]^{-1} \quad (24)$$

where $\mathbf{P}(n | n - 1)$ represents the previously predicted state error covariance matrix, and σ_ω^2 is the measurement noise covariance.

Recalling eq. (23), the Kalman gain matrix $\mathbf{K}(n)$ is used to correct the prediction by the appropriate amount. When a high Kalman gain is obtained, it means that the previous prediction is unreliable. When the Kalman gain is small, it means that the previous prediction is appropriate. The accurate estimation of Kalman gain is relevant to the predicted state error covariance matrix and measurement noise covariance. In practical application, the measurement noise covariance σ_ω^2 is a user-defined parameter and is related to the resolution of the fractional delay estimator in this paper.

3.3. Doppler Tracking

Once the currently estimated state vector $\hat{\mathbf{x}}(n | n)$ is obtained, the filtered Doppler estimate $\hat{\alpha}_n$ is calculated by

$$\hat{\alpha}_{n+1} = \hat{\mathbf{x}}(n | n)(2)/c \quad (25)$$

where $\hat{\mathbf{x}}(n | n)(i)$ represents the i th item of the state vector $\hat{\mathbf{x}}(n | n)$.

Since the correlation magnitude is sensitive to Doppler offset, a local reference signal generator compensates for the magnitude distortion adaptively. Naturally, the filtered Doppler estimate $\hat{\alpha}_n$ is used to generate the local reference signal for the next period. For the sake of reducing complexity and limitation of sampling rate, the local reference signal changes as follows in practical application:

$$\tilde{\alpha}_{n+1} = \arg \min_{\alpha \in \alpha} |\hat{\alpha}_{n+1} - \alpha| \quad (26)$$

where α is pre-stored local reference signal in memory and described as

$$\alpha = \{\alpha_{-K}, \dots, \alpha_0, \dots, \alpha_K\} = \left\{ -\frac{K\Delta v}{c}, \dots, 0, \dots, \frac{K\Delta v}{c} \right\} \quad (27)$$

where Δv denotes the Doppler searching step.

Table 2. Main Function: Kalman-based Doppler Tracking Algorithm

Initialization:	
$\tau_{pre} = 0$, // initialize delay prediction	
$\alpha = \{\alpha_{-K}, \dots, \alpha_0, \dots, \alpha_K\}$, // initialize α according to eq. (27)	
\mathbf{Q} , // initialize \mathbf{Q} according to eq. (14)	
σ_ω^2 , // initialize delay measurement error	
$\mathbf{P}(2 2)$, // initialize \mathbf{P} according to eq. (35)	
$\hat{\mathbf{x}}(2 2)$, // initialize $\hat{\mathbf{x}}$ according to eq. (36)	
<hr/>	
1: $[\tilde{\tau}_0, \tilde{\alpha}_0] = \arg \max_{\tau \in \tau, \alpha \in \alpha} \left \int_{-\infty}^{+\infty} r(t) s^*((1 + \alpha)t + \tau) dt \right $	
2: for $n = 0 : N - 2$ do	
3: $r_n(\tau) = r(\tau), \quad \tilde{\tau}_{n-1} + nT_b < \tau < \tilde{\tau}_{n-1} + (n+2)T_b$	
4: $s_{\tilde{\alpha}_n}(\tau) = \varphi((1 + \tilde{\alpha}_n)\tau) e^{j2\pi f_c(1 + \tilde{\alpha}_n)\tau}$	
5: $R_n(\tau) = r_n(\tau) * \text{conj}(s_{\tilde{\alpha}_n}(\tau))$	
6: $[\hat{\tau}_n, \hat{\tau}_{n+1}] = \text{findEvpPos}(R_n(\tau), \tilde{\tau}_{n-1})$	
7: $z(n) = \text{fracDelayEst}(R_n(\tau), \hat{\tau}_n, \hat{\tau}_{n+1}, \tau_{pre})$	
8: $\mathbf{K}(n) = \mathbf{P}(n n-1) \mathbf{H} [\mathbf{H} \mathbf{P}(n n-1) \mathbf{H}^T + \sigma_\omega^2]^{-1}$	
9: $\hat{\mathbf{x}}(n n) = \hat{\mathbf{x}}(n n-1) + \mathbf{K}(n) [z(n) - \mathbf{H}^T \hat{\mathbf{x}}(n n-1)]$	
10: $[\hat{\alpha}_{n+1}, \tilde{\alpha}_{n+1}] = \text{updateAlpha}(\hat{\mathbf{x}}(n n))$	
11: $b_n(\tau) = \text{LPF}(R_n(\tau) e^{-j2\pi f_c(1 + \tilde{\alpha}_n)\tau})$	
12: $[\hat{b}_n, \hat{b}_{n+1}] = [b_n(\tau = \hat{\tau}_n), b_n(\tau = \hat{\tau}_{n+1})]$	
13: $\phi_n = 2\pi(1 + \tilde{\alpha}_n) f_c (\hat{\alpha}_{n+1} - \tilde{\alpha}_n) T_b$	
14: $\hat{a}_n = \hat{b}_{n+1} \hat{b}_n^* e^{-j\phi_n}$	
15: $\mathbf{P}(n n) = [\mathbf{I} - \mathbf{K}(n) \mathbf{H}^T] \mathbf{P}(n n-1)$	
16: $\mathbf{P}(n+1 n) = \mathbf{A} \mathbf{P}(n n) \mathbf{A}^T + \mathbf{Q}$	
17: $\hat{\mathbf{x}}(n+1 n) = \mathbf{A} \hat{\mathbf{x}}(n n)$	
18: $\tau_{pre} = \mathbf{H} \hat{\mathbf{x}}(n+1 n)$	
19: end for	
<hr/>	
Subfunction: $[\hat{\tau}_n, \hat{\tau}_{n+1}] = \text{findEvpPos}(R_n(\tau), \tilde{\tau}_{n-1})$	
1: $\tau_n = \{\tau \tilde{\tau}_{n-1} + nT_b < \tau < \tilde{\tau}_{n-1} + (n+1)T_b\}$	
2: $\tau_{n+1} = \{\tau \tilde{\tau}_{n+1} + nT_b < \tau < \tilde{\tau}_{n-1} + (n+2)T_b\}$	
3: $\hat{\tau}_n = \arg \max_{\tau \in \tau_n} R_n(\tau) $	
4: $\hat{\tau}_{n+1} = \arg \max_{\tau \in \tau_{n+1}} R_n(\tau) $	
<hr/>	
Subfunction: $[\hat{\alpha}, \tilde{\alpha}_n] = \text{updateAlpha}(\hat{\mathbf{x}}(n n))$	
1: $\hat{\mathbf{x}} = \hat{\mathbf{x}}(n n)$	
2: $\hat{\alpha}_n = \hat{\mathbf{x}}(2)/c$	
3: $\tilde{\alpha}_n = \arg \min_{\alpha \in \alpha} \hat{a}_n - \alpha $	

3.4. Symbol Decision

Recalling the cross-correlation signal in eq. (20), the equivalent baseband signal that contains the transmitted symbol is calculated by

$$b_n(\tau) = \text{LPF}(R_n(\tau) e^{-j2\pi f_c(1 + \tilde{\alpha}_n)\tau}) \quad (28)$$

Symbol synchronization and decimation is realized accordingly by

$$[\hat{b}_n, \hat{b}_{n+1}] = [b_n(\tau = \hat{\tau}_n), b_n(\tau = \hat{\tau}_{n+1})] \quad (29)$$

where $\hat{\tau}_n, \hat{\tau}_{n+1}$ are obtained by eq. (22).

The estimate of transmitted information symbol is refined based on the filtered Doppler estimate as

$$\hat{a}_n = \hat{b}_{n+1} \hat{b}_n^* e^{-j\phi_n} \quad (30)$$

where ϕ_n denotes the residual phase rotation induced by the remaining Doppler offset, and is calculated by

$$\phi_n = 2\pi(1 + \tilde{\alpha}_n) f_c (\hat{\alpha}_{n+1} - \tilde{\alpha}_n) T_b \quad (31)$$

3.5. Delay Prediction

Once the Kalman gain is obtained, the state error covariance is updated by

$$\mathbf{P}(n | n) = [\mathbf{I} - \mathbf{K}(n)\mathbf{H}^T] \mathbf{P}(n | n - 1) \quad (32)$$

The state vector is predicted from the state dynamic equation by using

$$\hat{\mathbf{x}}(n + 1 | n) = \mathbf{A}\hat{\mathbf{x}}(n | n) \quad (33)$$

where $\hat{\mathbf{x}}(n + 1 | n)$ is the predicted state vector that contains the delay prediction for the next observation.

Next, the state error covariance matrix can also be predicted using

$$\mathbf{P}(n + 1 | n) = \mathbf{A}\mathbf{P}(n | n)\mathbf{A}^T + \mathbf{Q} \quad (34)$$

where \mathbf{Q} is the process noise covariance that controls the tolerance of model mismatch, and is defined by eq. (14).

To accelerate the convergence rate of the Kalman filter, the initialization of $\mathbf{P}(n|n)$ and $\hat{\mathbf{x}}(n|n)$ are given as [17]

$$\hat{\mathbf{x}}(2 | 2) = \begin{bmatrix} z(2) \\ \frac{c(z(2)-z(1))}{\Delta t} \\ \frac{c(z(2)+z(0)-2z(1))}{\Delta t^2} \end{bmatrix} \quad (35)$$

and

$$\mathbf{P}(2|2) = E\{\hat{\mathbf{x}}(2 | 2)\hat{\mathbf{x}}(2 | 2)^T\} = \begin{bmatrix} \sigma_\omega^2 & \frac{c\sigma_\omega^2}{\Delta t} & \frac{c\sigma_\omega^2}{\Delta t^2} \\ \frac{c\sigma_\omega^2}{\Delta t} & \frac{2c^2\sigma_\omega^2}{\Delta t^2} & \frac{3c^2\sigma_\omega^2}{\Delta t^3} \\ \frac{c\sigma_\omega^2}{\Delta t^2} & \frac{3c^2\sigma_\omega^2}{\Delta t^3} & \frac{6c^3\sigma_\omega^2}{\Delta t^4} \end{bmatrix} \quad (36)$$

where $z(0), z(1), z(2)$ denote the first three delay measurements.

To refine the delay estimate in eq. (21), the delay prediction contained in the predicted state vector is used and described as

$$\tau_{pre} = \mathbf{H}\hat{\mathbf{x}}(n + 1 | n) \quad (37)$$

3.6. Multiple Path Combination

Since differential detection is performed in the proposed algorithm, the energies of multiple paths are combined directly as

$$\hat{a}_n = \sum_{p=0}^{P-1} \hat{b}_{n+1,p} \hat{b}_{n,p}^* e^{-j\phi_{n,p}} \quad (38)$$

where $\hat{b}_{n,p}, \hat{b}_{n+1,p}$ denotes the baseband symbol for p th path, and $\phi_{n,p}$ denotes the corresponding phase rotation. Since a non-uniform path speed model is assumed, the Doppler tracking is performed for each path separately, and a combination of multipath diversity is performed after that.

To summarize, the proposed algorithm applies the fractional delay estimation of high resolution as the measurement of Kalman filter, produces filtered Doppler estimates to compensate the residual phase rotation, and mitigate correlation magnitude distortion. The delay prediction of the Kalman filter is used to refine the delay measurement. The step-by-step implementation of the proposed algorithm is summarized in Table 2.

4. Numerical Simulation

In this section, numerical simulation is conducted to illustrate the performance of the proposed Kalman-based Doppler tracking algorithm. Since the underwater acoustic channel is characterized as ultra-wideband and dynamic, the Doppler spread changes significantly within the transmission packet when its duration is sufficiently long, especially for the spread spectrum signal that modulates information bits with a long spread sequence. The CA model is

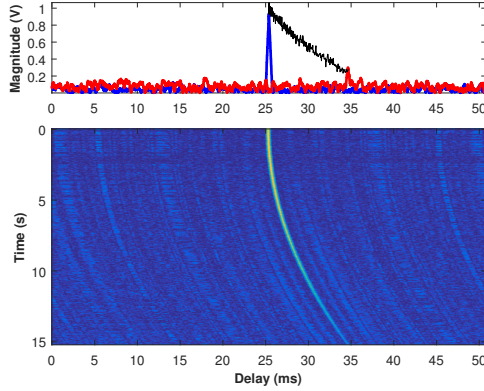


Figure 3. The power-delay-profile evolution of spread spectrum signal without Doppler tracking.

therefore addressed herein. Unless otherwise stated, the duration of the spread sequence is longer than the maximum delay spread of multipath.

In our simulation, a spread spectrum system of the DBPSK transmission scheme is considered. The spread sequence is in the form of m-sequence with a length of $L = 127$. The chip interval is $T_c = 0.4$ ms, the symbol interval $T_b = LT_c = 50.8$ ms, and the carrier frequency is $f_c = 12.5$ kHz. The received signal is sampled with the rate of $f_s = 100$ kHz. The length of transmitted differential encoded symbols is $N = 300$, and the duration of the transmitted signal is $T = NT_b = 15.24$ s. The underwater sound speed is assumed to be $c = 1500$ m/s.

4.1. Case 1: Single Path With Constant Acceleration

We consider a single path channel where Doppler is modeled as constant acceleration (CA) [18, 19]

$$h(t, \tau) = h_0 \delta(\tau - \tau_0(t)) \quad (39)$$

where $h_0 = 1$ denotes the constant magnitude, and

$$\tau_0(t) = \tau_0 + \frac{a_0 t^2}{2c} \quad (40)$$

where $\tau_0 = d_0/c$ denotes the initial transmission delay from the transmitter to the receiver, and $a_0 = 0.12$ m/s² denotes the acceleration speed. A total of $2K + 1$ local reference signals are stored in the memory for compensating magnitude distortion, and its Doppler offset is described as

$$\alpha = \left\{ -\frac{K\Delta v}{c}, \dots, 0, \dots, \frac{K\Delta v}{c} \right\} \quad (41)$$

where $K = 10$, and $\Delta v = 0.3$ m/s. The parameters used for Kalman filter initialization are set as $\sigma_\omega = 1$ us, and $\sigma_g = 0.02$ m/s³.

Fig. 3 and Fig. 4 show the power-delay-profile (PDP) evolution of spread spectrum signal and its magnitude intensity of received symbols with and without Doppler tracking, and Fig. 5 compares the correlation magnitude for the two methods. In this case, the signal-to-noise ratio of each symbol, i.e., E_s/N_0 , is set to 30 dB. As shown, each symbol's arrival time changes obviously along with the delay axis induced by the Doppler spread. The magnitude of received symbols decreases dramatically along the time axis when the local reference signal is fixed. When the proposed Kalman-based Doppler tracking algorithm is performed, the magnitude of received symbols remains nearly constant along the time axis. The results indicate that dynamic Doppler tracking is essential for spread-spectrum communications, especially when Doppler spread changes significantly within the data packet.

Three Doppler tracking algorithms suitable for spread spectrum signals are compared in this scenario. The first method is the proposed Kalman-based Doppler tracking algorithm (KBDT). The second is the symbol-based passband

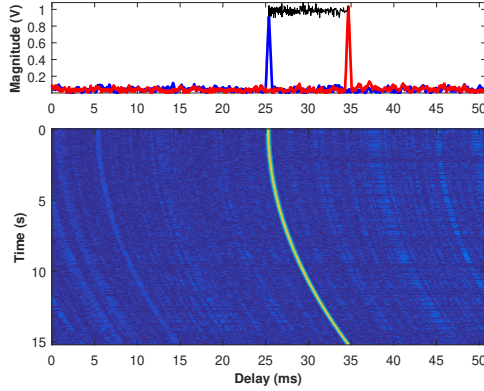


Figure 4. The power-delay-profile evolution of spread spectrum signal with Doppler tracking.

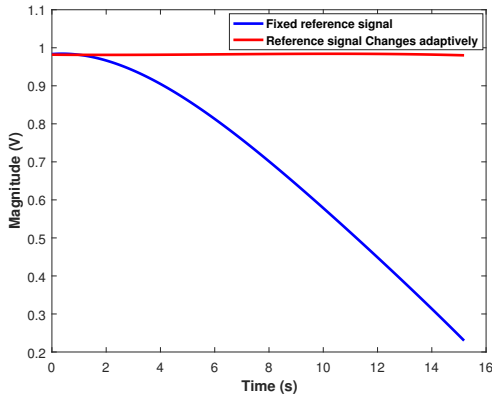


Figure 5. The correlation magnitude of received symbols with and without Doppler tracking.

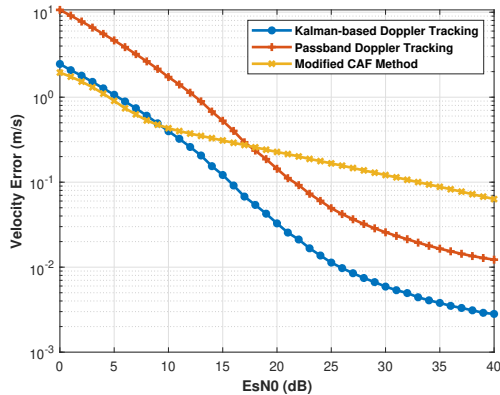


Figure 6. Resolution of Doppler estimates with different Doppler tracking algorithms

Doppler tracking (PBDT) algorithm without Kalman filtering [10], and the third is the modified CAF method [8]. Fig. 6 shows the Doppler resolution of the three mentioned Doppler tracking algorithms. As shown, the proposed

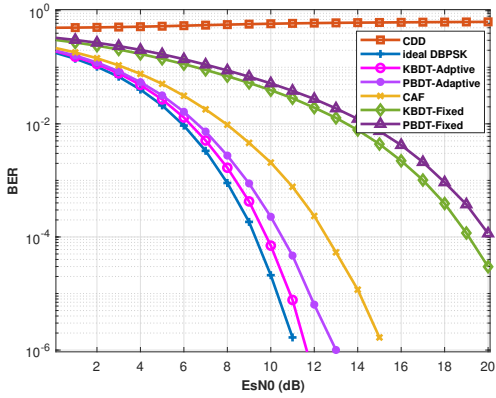


Figure 7. BER performance comparison of different receivers where the channel is modeled as a single path with constant acceleration

KBDT has a higher resolution of Doppler estimation compared with the PBDT and the modified CAF method. The modified CAF method has a higher resolution than the other two methods when SNR is low, whereas the computation complexity is high.

As shown in Fig. 7, in addition to the three methods mentioned above, the conventional differential detection method that makes symbol decisions without Doppler tracking and compensation (CDD), the proposed KBDT algorithm with a fixed reference signal (KBDT-Fixed), and PBDT algorithm with a fixed reference signal (PBDT-Fixed) is considered here to evaluate the BER performance. The KBDT-Adaptive and PBDT-Adaptive are used to distinguish their fixed version in the chart, i.e., KBDT-Fixed and PBDT-Fixed, respectively. These six methods are compared to the ideal DBPSK performance, where distortion of magnitude and phase rotation is removed. As shown, the conventional detection is invalid in this case due to the dramatic change of Doppler within the data packet. Compared with the modified CAF method, the performance gain of the PBDT method is around 2 dB, while the performance gain of the KBDT method is around 3 dB. The BER performance of the KBDT is close to the ideal DBPSK performance, where the performance loss is less than 0.5 dB. Compared with the KBDT-Fixed method, the proposed KBDT method has a performance gain of around 9 dB by changing the local reference signal adaptively. Moreover, the PBDT method has the same performance gain compared with its fixed version (PBDT-Fixed).

4.2. Case 2: Multiple Path With Sinusoidal Fluctuant Surface

In this scenario, we consider the multiple paths with a sinusoidal fluctuant surface where the transmitter and receiver are fixed [20].

$$h(t, \tau) = \sum_{p=0}^{P-1} h_p \delta(\tau - \tau_p(t)) \quad (42)$$

where $P = 3$, $[h_0, h_1, h_2] = [0.707, 0.5, 0.5]$, $\tau_0(t) = 25$ ms, $\tau_1(t) = \tau_0 + 5$ ms, and

$$\tau_2(t) = \tau_2 + \frac{d_2}{c} \sin(2\pi f_2 t) \quad (43)$$

where $\tau_2 = \tau_0 + 7$ ms, $d_2 = 0.3$ m denotes the surface drifting range, and $f_2 = 0.2$ Hz denotes the surface drifting frequency.

Fig. 8 shows the PDP evolution of spread spectrum signal with channel model as sinusoidal fluctuant surface. Path 0 denotes the direct arrival without reflection, path 1 denotes the reflected sound coming from the bottom, and path 2 denotes the reflected sound coming from the surface. In this case, the assumption that models the channel with constant acceleration is unsuitable, resulting in a model mismatch of the Kalman filter.

Fig. 9 shows the Doppler estimation error with different σ_g . As shown, the Doppler estimation error decreases with increasing σ_g . Recalling eq. (14), the process noise covariance matrix \mathbf{Q} increases subsequently with the increase

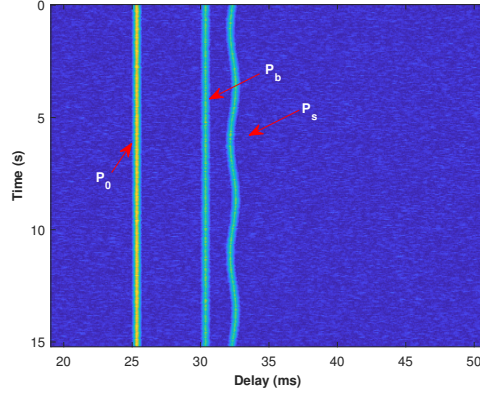


Figure 8. The PDP evolution of spread spectrum signal where the channel is modeled as multiple paths with the sinusoidal fluctuant surface.

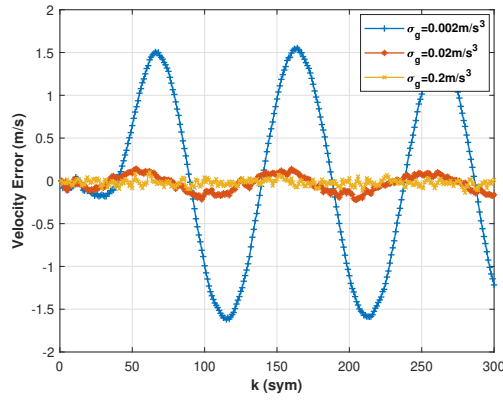


Figure 9. Doppler estimation error with different Kalman parameters for path 2.

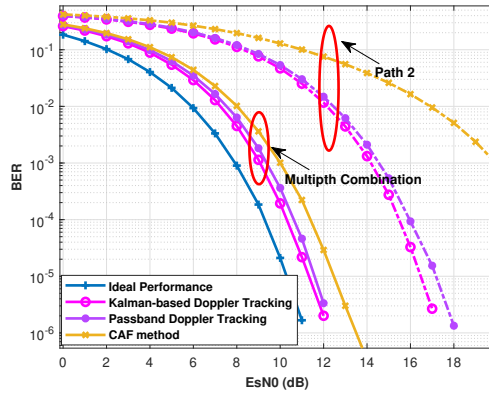


Figure 10. BER performance comparison of different receivers where the channel is modeled as multiple paths with the sinusoidal fluctuant surface.

of σ_g , and the tolerance to model error increases. In such a channel, it is not reasonable to take the value of σ_g as 0.02m/s^3 , and it should be taken as 0.2m/s^3 .

BER performance of the proposed Kalman-based Doppler tracking algorithm is presented in Fig. 10. As shown,

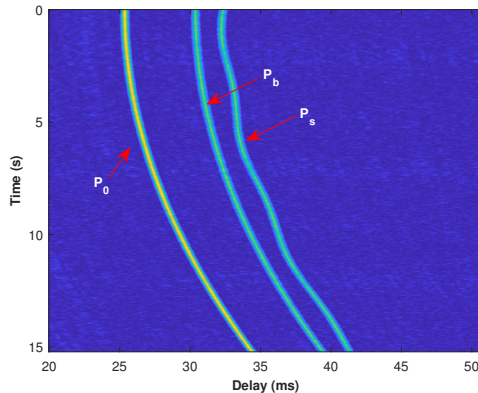


Figure 11. The PDP evolution of spread spectrum signal. The channel is described as multipath with a sinusoidal fluctuant surface where motion between the transmitter and receiver is modeled by constant acceleration.

the BER performance of the CAF method is nearly close to the proposed algorithm and the passband Doppler tracking algorithm. Path 0 and path 1 are described with static additive Gaussian channels without Doppler spread. The difference in BER performance comes from the surface path, i.e., path 2. For path 2, the proposed algorithm has a performance gain of 6dB compared to the CAF method.

4.3. Case 3: Multiple Path With Constant Acceleration and Sinusoidal Fluctuant Surface

Case 1 and Case 2 are combined in this scenario. The channel is described as multipath with a sinusoidal fluctuant surface where motion between the transmitter and receiver is modeled by constant acceleration.

$$h(t, \tau) = \sum_{p=0}^{P-1} h_p \delta(\tau - \tau_p(t)) \quad (44)$$

where

$$\tau_p(t) = \tau_p + \frac{a_p t^2}{2c} + \frac{d_p}{c} \sin(2\pi f_p t) \quad (45)$$

where $P = 3$, $[h_0, h_1, h_2] = [0.707, 0.5, 0.5]$, $[\tau_0, \tau_1, \tau_2] = [25, 30, 32]$ ms, $a_0 = a_1 = a_2 = 0.12 \text{ m/s}^2$, $d_0 = d_1 = 0 \text{ m}$, $f_0 = f_1 = 0 \text{ Hz}$, $d_2 = 0.3 \text{ m}$, and $f_2 = 0.2 \text{ Hz}$.

The parameters used for Kalman filter initialization are set as $\sigma_\omega = 1 \text{ us}$, and $\sigma_g = 0.02 \text{ m/s}^3$ for path 0 and path 1. σ_g is set as 0.2 m/s^3 for path 2 according to the simulation results in Case 2.

Fig. 11 shows the corresponding PDP evolution of spectrum signal with the proposed Kalman-based Doppler tracking algorithm. The proposed algorithm is able to track the variation of Doppler spread under such a channel. As shown in Fig. 12, the BER performance of the proposed algorithm is close to the ideal performance of the DBPSK system, and has a performance gain of around 1 dB to the passband Doppler tracking algorithm, and around 4 dB to the CAF method.

5. Experimental Data Analysis

A set of data collected from the Songhua Lake, Jilin, China, on Oct. 28th, 2019, is used to evaluate the performance of the proposed algorithm. Fig. 13 shows the system configuration of the acoustic testing. As shown, the transmitter is fixed at the station near the shore with a deployed depth of 2 m. A receiving array of 5-element hydrophones is fixed on the moving boat with a deployed depth of 2 m. The depth of the working area ranges from 30 to 50 m. The boat moves along the trajectory as shown, where the farthest distance is around 2.8 km.

The signal is in the form of DS-SS-DBPSK with $N = 290$ symbols. The spread sequence is in the form of m-sequence with a length of $L = 127$, where the corresponding spread gain is $G = 21 \text{ dB}$. The chip interval is $T_c = 0.4$

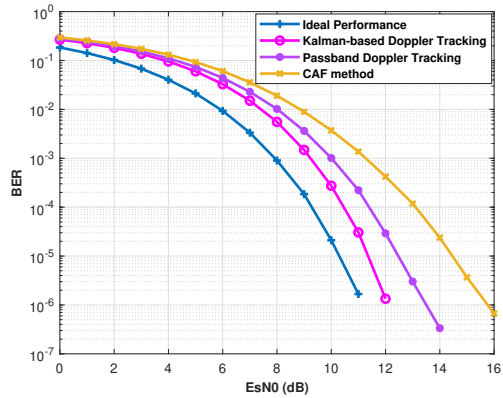


Figure 12. BER performance comparison of different receivers where the channel is described as multipath with a sinusoidal fluctuant surface where motion between the transmitter and receiver is modeled by constant acceleration.

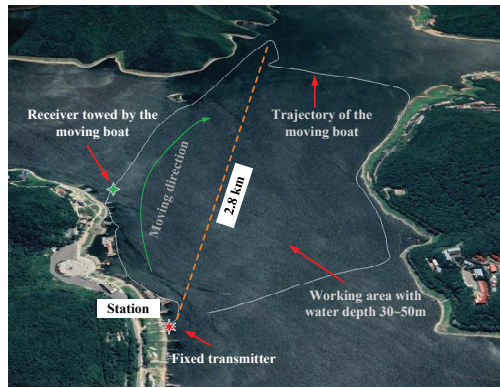


Figure 13. System setup of the acoustic field testing.

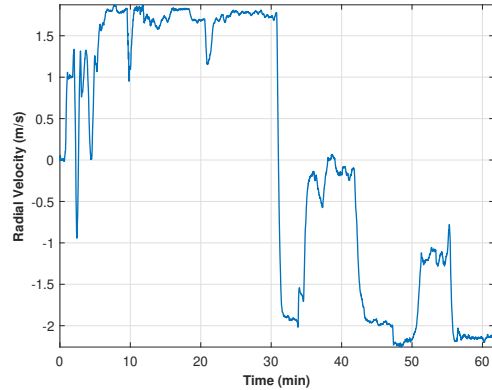


Figure 14. Radial velocities measured with differential GPS.

ms, the symbol interval $T_b = LT_c = 50.8$ ms and the carrier frequency is $f_c = 12.5$ kHz. The received signal is sampled with a rate of $f_s = 100$ kHz. The duration of transmitted signal is $T = NT_b = 14.732$ s. Fig. 14 shows the radial velocities of transmitter and receiver measured with differential GPS over time.

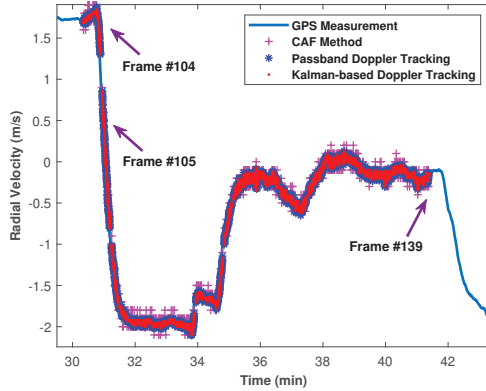


Figure 15. The Doppler estimation results of different methods.

5.1. Test 1: Doppler Tracking in Variable Speed Motion Scenario

As shown in Fig. 14, the largest change in velocity occurs at around 30 min. The acquired signals from this nearby time period are used to evaluate the proposed Kalman-based Doppler tracking algorithm. The parameters used for the proposed algorithm's initialization are set as $K = 20$, $\Delta v = 0.1 \text{ m/s}$, $\sigma_\omega = 1 \text{ us}$, and $\sigma_g = 0.2 \text{ m/s}^3$.

The CAF method (CAF) with Doppler step size of 0.1 m/s, the passband Doppler tracking algorithm (PBDT), and the proposed Kalman-based Doppler tracking algorithm (KBDT) are evaluated in this test. Fig. 15 shows the Doppler estimation results from 30 min to 42 min of the three methods, and are compared with the radial velocity measurement of GPS. As shown, all three methods are able to track the variation of the Doppler offset nicely. The proposed Kalman-based Doppler tracking algorithm has the smallest variance of the estimates, and the CAF method has the largest.

The average input SNR of the signal ranges from 4 dB to 8 dB during this time period, and the corresponding output SNR ranges from 25 dB to 29 dB. The input SNR of the received signal is measured based on the synchronized symbols, $\hat{\mathbf{b}} = \{\hat{b}_n\}$, and is calculated as

$$\text{SNR}_{in} = 20 \lg \frac{\text{mean}\{\|\hat{\mathbf{b}}\|\}}{\text{std}\{\|\hat{\mathbf{b}}\|\}} - G \quad (46)$$

where G is the spread gain.

Specifically, the signal of frame #105 is addressed in our discussion. In this data frame, the Doppler variation of the signal is drastic, and is approximated as constant acceleration. Fig. 16 shows the PDP evolution of the spread spectrum signal in this frame, where the local reference signal is fixed. The multipath consists of a stable direct path and two reflected paths with little energy, and the maximum delay spread is around 1 ms. The magnitude of correlation output decreases along with the packet due to Doppler variation.

The noise acquired from the experiment is added to the signal of frame #105 to evaluate the BER performance of the proposed algorithm. The input SNR of this frame signal is around 4 dB. The input SNR of the signal combined with the noise signal is calculated as

$$\text{SNR} = 10 \lg \frac{\alpha_1 \alpha_2}{\alpha_1 + \alpha_2} \quad (47)$$

where $\text{SNR}_{in} = 10 \lg \alpha_1$, and $\text{SNR}_{add} = 10 \lg \alpha_2$ denotes the ratio of the variance of the acquired signal to the variance of the noise signal.

Fig. 17 shows the corresponding BER performance of different methods. Note that the x-axis denotes the SNR of each symbol, i.e., the output SNR of the despreaded signal. The performance gain of the proposed algorithm with changing the local reference signal adaptively (KBDT-Adaptive) is around 3 dB compared with a fixed local reference signal (KBDT-fixed). In comparison, the passband Doppler tracking algorithm (PBDT-Adaptive) is around

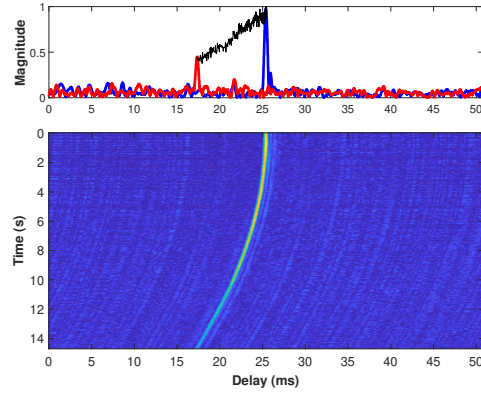


Figure 16. The PDP evolution of spread spectrum signal in the frame of #105, when the local reference signal is fixed.

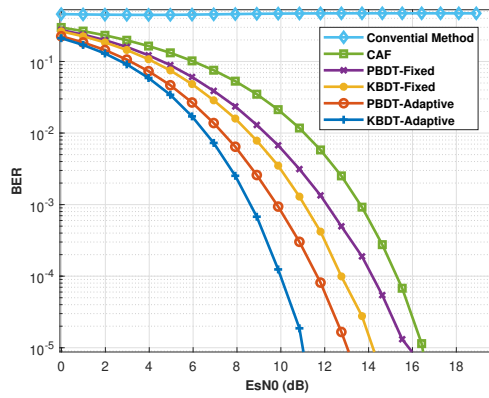


Figure 17. BER performance comparison of different methods where the channel is approximated as constant acceleration.

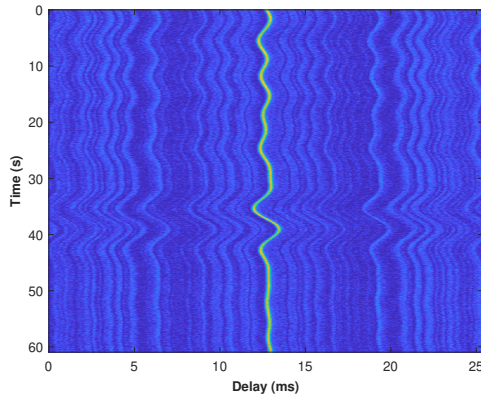


Figure 18. The PDP evolution of spread spectrum signal where the Doppler spread is caused by the fluctuant surface.

2 dB compared with its fixed version (PBDT-fixed). The conventional differential detection (CDD) is not valid in this case. The KBDT-Adaptive method has a performance gain of around 5 dB compared with the CAF method.

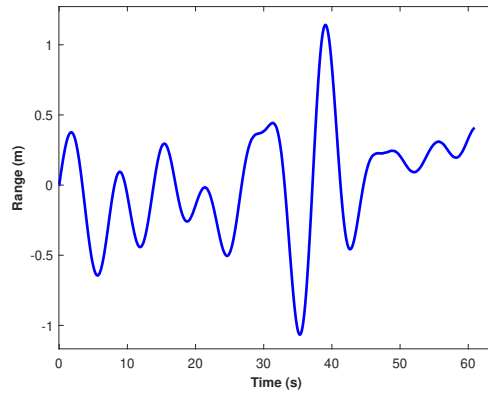


Figure 19. Variation of the transceiver radial distance caused by fluctuant surface.

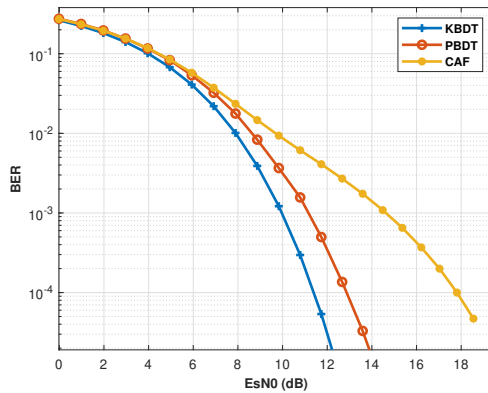


Figure 20. BER performance comparison of different methods where the Doppler spread is caused by the fluctuant surface.

5.2. Test 2: Doppler Tracking with Sinusoidal Fluctuant Surface

Fig. 18 shows the PDP evolution of the spread spectrum signal where the Doppler spread is induced by the sinusoidal fluctuant surface. In this case, the transmitter is fixed in the ocean bottom, and the receiver is fixed on the floating vessel. The chip interval is $T_c = 0.4$ ms, the length of fixed-emission symbols is $N = 2400$, and other parameters are the same as Test 1. As shown in Fig. 19, the corresponding variation of the transceiver radial distance induced by fluctuant surface ranges from 0.5 m to 1.0 m. The frequency of the fluctuant surface approximated by the cosine function is around 0.15 Hz.

Fig. 20 shows the BER performance of the KBDT, PBDT, and CAF methods. As shown, the performance gain of the KBDT method is around 6 dB compared with the CAF method and around 1.5 dB compared with the PBDT method. In this case, the performance of KBDT and PBDT are the same as KBDT-Fixed and PBDT-Fixed, respectively, due to the reference signal are the same for the data packet.

6. Conclusion

An algorithm that dynamically tracks and compensates the Doppler spread of DSSS signal is addressed for underwater acoustic spread spectrum communications in this paper. The Doppler spread is manifested as frequency shifting and time scaling. An accurate delay estimation of high accuracy is performed by fully using the potential of passband signal of high sampling rate and utilizing fractional time delay estimator. A Kalman filter converts the delay estimates into instant filtered Doppler estimates based on the delay-Doppler equation. Both magnitude distortion and phase

rotation of the received signal are corrected by adaptively changing local reference signal and phase compensation. Simulation results demonstrate that the performance of the proposed algorithm is closed to the ideal DBPSK system. The proposed algorithm is able to track the Doppler variation where the channel is modeled as constant acceleration and sinusoidal surface. It is concluded that dynamic Doppler tracking and compensation are essential for underwater spread spectrum communications, especially when the Doppler changes significantly within a data packet. The processing results of the experimental data also demonstrate that the proposed algorithm is able to track the Doppler variation within the packet and mitigate the magnitude distortion and phase rotation.

References

- [1] T. Yang, W.-B. Yang, Performance analysis of direct-sequence spread-spectrum underwater acoustic communications with low signal-to-noise-ratio input signals, *The Journal of the Acoustical Society of America* 123 (2) (2008) 842–855.
- [2] T. Yang, W.-B. Yang, Interference suppression for code-division multiple-access communications in an underwater acoustic channel, *The Journal of the Acoustical Society of America* 126 (1) (2009) 220–228.
- [3] M. Stojanovic, J. Preisig, Underwater acoustic communication channels: Propagation models and statistical characterization, *IEEE communications magazine* 47 (1) (2009) 84–89.
- [4] T. Yang, Properties of underwater acoustic communication channels in shallow water, *The Journal of the Acoustical Society of America* 131 (1) (2012) 129–145.
- [5] P. Hursky, M. B. Porter, M. Siderius, V. K. McDonald, Point-to-point underwater acoustic communications using spread-spectrum passive phase conjugation, *The Journal of the Acoustical Society of America* 120 (1) (2006) 247–257.
- [6] M. Stojanovic, L. Freitag, Hypothesis-feedback equalization for direct-sequence spread-spectrum underwater communications, in: OCEANS 2000 MTS/IEEE Conference and Exhibition. Conference Proceedings (Cat. No. 00CH37158), Vol. 1, IEEE, 2000, pp. 123–129.
- [7] R. Diamant, A. Feuer, L. Lampe, Choosing the right signal: Doppler shift estimation for underwater acoustic signals, in: Proceedings of the Seventh ACM International Conference on Underwater Networks and Systems, 2012, pp. 1–8.
- [8] S. M. Kay, S. B. Doyle, Rapid estimation of the range-doppler scattering function, *IEEE Transactions on Signal Processing* 51 (1) (2003) 255–268.
- [9] T. Yang, W.-B. Yang, Low probability of detection underwater acoustic communications using direct-sequence spread spectrum, *The Journal of the Acoustical Society of America* 124 (6) (2008) 3632–3647.
- [10] D. Sun, X. Hong, H. Cui, L. Liu, A symbol-based passband doppler tracking and compensation algorithm for underwater acoustic dsss communications, *Journal of Communications and Information Networks* 5 (2) (2020) 168–176.
- [11] R. Wu, J. Li, Time-delay estimation via optimizing highly oscillatory cost functions, *IEEE Journal of Oceanic Engineering* 23 (3) (1998) 235–244.
- [12] F. Qu, Z. Wang, L. Yang, Z. Wu, A journey toward modeling and resolving doppler in underwater acoustic communications, *IEEE Communications Magazine* 54 (2) (2016) 49–55.
- [13] X. Xu, Z. Wang, S. Zhou, L. Wan, Parameterizing both path amplitude and delay variations of underwater acoustic channels for block decoding of orthogonal frequency division multiplexing, *The Journal of the Acoustical Society of America* 131 (6) (2012) 4672–4679.
- [14] C. M. G. Gussen, R. S. Chaves, P. S. R. Diniz, W. A. Martins, Doppler effects on transceivers with reduced redundancy, in: 2015 IEEE International Conference on Digital Signal Processing (DSP), 2015, pp. 388–392. doi:10.1109/ICDSP.2015.7251899.
- [15] M. B. Rhudy, R. A. Salguero, K. Holappa, A kalman filtering tutorial for undergraduate students, *International Journal of Computer Science & Engineering Survey* 8 (1) (2017) 1–18.
- [16] I. Céspedes, Y. Huang, J. Ophir, S. Spratt, Methods for estimation of subsample time delays of digitized echo signals, *Ultrasonic imaging* 17 (2) (1995) 142–171.
- [17] H. You, X. Jianjuan, G. Xin, Radar data processing with applications, John Wiley & Sons, 2016.
- [18] T. J. Riedl, A. C. Singer, Broadband doppler compensation: Principles and new results, in: 2011 Conference Record of the Forty Fifth Asilomar Conference on Signals, Systems and Computers (ASILOMAR), IEEE, 2011, pp. 944–946.
- [19] Y. Zakharov, J. Li, Autocorrelation method for estimation of doppler parameters in fast-varying underwater acoustic channels, in: Underwater Acoustics, Conference and Exhibition, UACE-2015. Crete, Greece, 2015, pp. 1–4.
- [20] M. Siderius, M. B. Porter, Modeling broadband ocean acoustic transmissions with time-varying sea surfaces, *The Journal of the Acoustical Society of America* 124 (1) (2008) 137–150.